ADAMTS-1: a metalloproteinase-disintegrin essential for normal growth, fertility, and organ morphology and function

Takayuki Shindo,[1] Hiroki Kurihara,[1,2] Kouji Kuno,[2,3] Hitoshi Yokoyama,[4] Takashi Wada,[5] Yukiko Kurihara,[1] Tomihiko Imai,[1] Yuhui Wang,[1] Masafumi Ogata,[3] Hiroaki Nishimatsu,[6] Nobuo Moriyama,[6] Yoshio Oh-hashi,[1] Hiroyuki Morita,[1] Takatoshi Ishikawa,[7] Ryozo Nagai,[1] Yoshio Yazaki,[8] and Kouji Matsushima[2,9]

[1]Department of Cardiovascular Medicine, Graduate School of Medicine, University of Tokyo, Tokyo, Japan
[2]Core Research for Evolutional Science and Technology (CREST), Japan Science and Technology Corporation, Tokyo, Japan
[3]Department of Molecular Pharmacology, Cancer Research Institute,
[4]Division of Blood Purification, and
[5]First Department of Internal Medicine, School of Medicine, Kanazawa University, Kanazawa, Japan
[6]Department of Urology, and
[7]Department of Pathology, Graduate School of Medicine, University of Tokyo, Tokyo, Japan
[8]The Hospital International Medical Center of Japan, Tokyo, Japan
[9]Department of Molecular Preventive Medicine, Graduate School of Medicine, University of Tokyo, Tokyo, Japan

Address correspondence to: Hiroki Kurihara, Department of Cardiovascular Medicine, Graduate School of Medicine, University of Tokyo, 7-3-1 Hongo, Bunkyo-ku, Tokyo 113-8655, Japan. Phone: 81-3-5800-6519; Fax: 81-3-5800-8824; E-mail: kuri-tky@umin.ac.jp.

Takayuki Shindo, Hiroki Kurihara, and Kouji Kuno contributed equally to this work.

Received for publication October 7, 1999, and accepted in revised form March 17, 2000.

A disintegrin and metalloproteinase (ADAM) represents a protein family possessing both metalloproteinase and disintegrin domains. ADAMTS-1, an ADAM family member cloned from cachexigenic colon adenocarcinoma, is unusual in that it contains thrombospondin type I motifs and anchors to the extracellular matrix. To elucidate the biological role of ADAMTS-1, we developed *ADAMTS-1*–null mice by gene targeting. Targeted disruption of the mouse *ADAMTS-1* gene resulted in growth retardation with adipose tissue malformation. Impaired female fertilization accompanied by histological changes in the uterus and ovaries also resulted. Furthermore, *ADAMTS-1*$^{-/-}$ mice demonstrated enlarged renal calices with fibrotic changes from the ureteropelvic junction through the ureter, and abnormal adrenal medullary architecture without capillary formation. ADAMTS-1 thus appears necessary for normal growth, fertility, and organ morphology and function. Moreover, the resemblance of the renal phenotype to human ureteropelvic junction obstruction may provide a clue to the pathogenesis of this common congenital disease.

J. Clin. Invest. **105**:1345–1352 (2000).

Introduction

Proteolytic modification of cell-surface proteins and extracellular matrices is pivotal for a diverse array of biological and pathological processes, including embryogenesis, wound healing, and cancer metastasis. A disintegrin and metalloproteinase (ADAM) represents a protein family possessing both metalloproteinase and disintegrin domains. Recently, the ADAM protein family has emerged as a key participant in these processes (1, 2). More than 20 proteins have been identified as members of the ADAM family. Fertilin-α/β, the first ADAM described, has been implicated in integrin-mediated sperm-egg binding (3, 4). Subsequently, meltrin-α was shown to be involved in muscle fusion (5). TNF-α–converting enzyme, which cleaves the membrane-anchored precursor of TNF-α, thus upregulating production of TNF-α, has recently proved to be a member of the ADAM family (6–9). In the fruit fly *Drosophila*, an ADAM family gene called Kuzbanian has been demonstrated to play a role in lateral inhibition during neurogenesis by coding for cleavage of the extracellular domain of the transmembrane receptor Notch (10, 11). Despite accumulating findings about the biological role of these ADAM proteins, the respective functions of the growing number of ADAM family members remain largely unknown.

ADAMTS-1 is a new member protein of the ADAM family, which was originally identified by differential display analysis as a gene highly expressed in the murine colon 26 cachexigenic tumor (12). In vivo expression of the gene is induced in the kidney and heart of mice treated with LPS, suggesting a possible role of ADAMTS-1 in the inflammatory reaction (12). Whereas typical ADAMs are membrane-anchored proteins that have a transmembrane region in the car-

boxyl-terminal region, ADAMTS-1 does not contain a transmembrane domain, but possesses three thrombospondin type I motifs at its carboxyl terminus, which are conserved motifs in both thrombospondin 1 and 2 (12, 13). After secretion, ADAMTS-1 is incorporated into the extracellular matrix. Site-directed mutagenesis revealed that these thrombospondin type I motifs, together with the carboxyl-terminal spacing region, are responsible for anchoring to the extracellular matrix (14). Recent studies using α2-macroglobulin as a substrate demonstrated that the metalloproteinase domain of ADAMTS-1 is functional (15). Thus, ADAMTS-1 is an active ADAM protease that is closely associated with the extracellular matrix, although its physiological substrate or substrates remain unclear.

Recent reports have identified several proteins whose structures are highly similar to ADAMTS-1. Procollagen I N-proteinase and aggrecanase-1/ADAMTS-4, which are involved in collagen maturation and proteoglycan degradation, respectively, possess thrombospondin type I motifs as well as disintegrin and metalloproteinase domains (16–18). METH-1, a human orthologue of ADAMTS-1, and METH-2 have been shown to inhibit FGF-2–induced vascularization in the cornea pocket assay, and to inhibit VEGF-induced angiogenesis in the chorioallantoic membrane assay (19). Furthermore, GON-1, a metalloproteinase that controls gonadogenesis by remodeling basement membranes in *Caenorhabditis elegans*, also demonstrates a structural similarity to ADAMTS-1 (20). Thus, these proteins appear to constitute a subfamily of ADAM (21), and the widely conserved structure among organisms ranging from *C. elegans* to humans leads us to suppose that their veiled biological functions are fundamental to life. To uncover the physiological and pathophysiological roles of ADAMTS-1 and gain insight into the biology of the ADAMTS protein family, we chose a gene-targeting strategy in mice. Here we show the multiple roles for ADAMTS-1 in normal growth, fertility, and organ structure and function.

Methods

Generation of ADAMTS-1–null mice. A 12.0-kb fragment spanning exons 1–7 of the mouse *ADAMTS-1* gene was subcloned into pBluescript (Stratagene, La Jolla, California, USA). The targeting vector was constructed by replacing the 1.6-kb *Eco*RI-*Bgl*II fragment encompassing exons 2–4 with the neomycin-resistance gene and flanking the thymidine kinase gene. This plasmid was linearized with *Not*I and introduced into 129/Sv–derived SM-1 embryonic stem (ES) cells by electroporation. The ES cells were selected in medium containing G418 and ganciclovir. Homologous recombinants were identified by PCR and Southern blot analysis. Two independently targeted ES cell clones were injected into C57BL/6 blastocysts to generate chimeric mice. Male chimeras were then crossbred with C57BL/6 females, and germline transmission was obtained from the two independent ES clones. Littermates obtained by breeding heterozygotes with the genetic background of the 129/Sv × C57BL/6 hybrid were used for phenotypic analysis.

RT-PCR. Total RNA was prepared from kidneys using RNAzol (BIOTEX), and RT-PCR was performed on the resultant cDNA samples. Primer sets were chosen as shown in Figure 1a, top; and sequences are as follows:

(a) Sense primer 5′-CGCTTCCATAACAATGCTGC-3′ and antisense primer 5′-CCTCAGGATGTGGAACTGCG-3′ were chosen within exon 1.

(b) Sense primer 5′-CGCAGTTCCACATCCTGAGG-3′ was chosen within exon 1, and antisense primer 5′-GCTGGACACAAATCGCTTCT-3′ was chosen within exon 2.

(c) Sense primer 5′-CAGGAAGCATAAGGAAGAAG-3′ was chosen within exon 2, and antisense primer 5′-GGCTTGTCCATCAAACATTC-3′ was chosen within exon 5.

(d) Sense primer 5′-CAGGAAGCATAAGGAAGAAG-3′ was chosen within exon 2, and antisense primer 5′-GCACAGTGCTTAGCATCATC-3′ was chosen within exon 4.

(e) Sense primer 5′-TTTTCAGAGTCTGGCAGAAG-3′ and antisense primer 5′-TGAGATGAGTGATCACCATG-3′ were chosen within exon 9. Thirty cycles (95°C for 1 minute, 62°C for 1 minute, 72°C for 1 minute) were used to amplify the products, which were then subjected to electrophoresis.

Histological examination. Specimens of kidney, adrenal gland, uterus, and ovary were fixed in 10% phosphate-buffered formalin (pH 7.4), embedded in paraffin, and cut into 4-μm sections. The sections were stained with hematoxylin and eosin or Mallory-azan and examined under light microscopy.

Uterus and ovaries were taken after 24 hours of treatment (subcutaneously) with 0.1 μg 17-β-estradiol.

Immunohistochemistry. Paraffin-embedded kidney tissue sections were dewaxed with Histo-Clear (National Diagnostics, Tokyo, Japan) and rehydrated with graded concentrations of ethanol. After blocking with avidin, biotin, and 1% skim milk, tissue sections were incubated with polyclonal antibodies against either the metalloproteinase domain of the mouse ADAMTS-1 protein or normal rabbit IgG overnight at 4°C. The sections were rinsed and then incubated for 30 minutes with biotinylated swine anti-rabbit Ig (1:400 dilution) (DAKO, Copenhagen, Denmark). The tissue sections were then rinsed and incubated for 30 minutes with alkaline phosphatase–labeled streptavidin (1:70 dilution). The slides were rinsed again in PBS and reacted with alkaline phosphatase substrate solution (Vector Laboratories, Burlingame, California, USA) containing 1 mM levamisole for 30 minutes at room temperature. Finally, the sections were rinsed and counterstained with methyl green.

Electron microscopy. Small parts of specimens were fixed with glutaraldehyde and osmium tetroxide, and then embedded in Epon 812 (Oken Shoji Co., Tokyo, Japan). From these embedded tissues, 0.1-μm sections were cut, double-stained with uranyl acetate or phosphotungstic

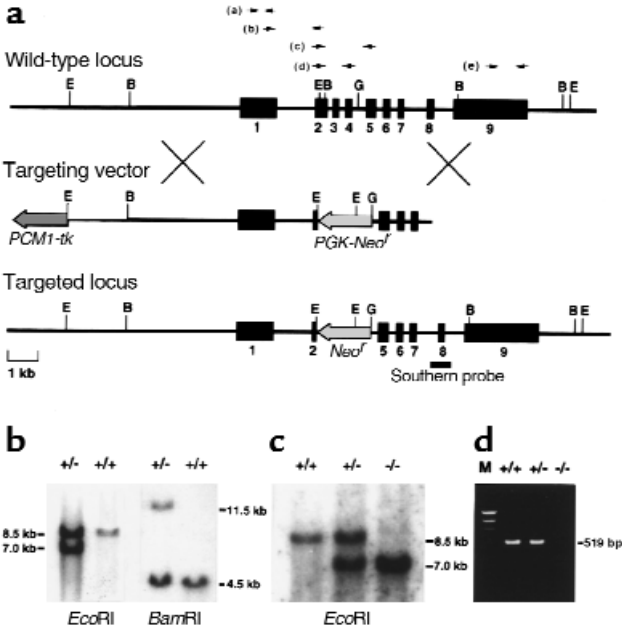

Figure 1
Targeted disruption of the mouse *ADAMTS-1* gene. (**a**) Genomic locus, targeting vector, and predicted targeted locus. Black boxes represent exons 1–9. The probe for Southern analysis is indicated. B, *Bam*HI; E, *Eco*RI; G, *Bgl*II. (**b** and **c**) Southern analysis of genomic DNA from targeted ES cells (**b**) and the offspring from a heterozygote intercross (**c**). The 7.0-kb *Eco*RI fragment and the 11.5-kb *Bam*HI fragment denote the homologous recombinant allele. (**d**) RT-PCR of total RNA extracted from the kidney of each genotype. No *ADAMTS-1* expression is detected in *ADAMTS-1*$^{-/-}$ mice.

acid and lead citrate, and examined with a Hitachi H-600 electron microscope (Hitachi Co., Tokyo, Japan).

Intravenous pyelography. After inducing anesthesia with intraperitoneal pentobarbital, 0.1 mL of radiopaque agent (meglumine sodium amidotrizoate) diluted to 1:1 with sterile saline was injected into the tail vein of each mouse. X-ray films were taken at 5, 10, 15, and 30 minutes after injection.

Statistical analysis. Quantitative values were expressed as mean ± SEM. The Student's *t* test was used to determine significant differences. A value of $P < 0.05$ was considered significant.

Results

Generation of ADAMTS-1–null mice. A targeting DNA construct was designed to replace exons 2–4, which encode most of the metalloproteinase domain (12, 13), with the neomycin-resistance gene (Figure 1a). The targeting vector was introduced into 129/Sv–derived ES cells by electroporation, and targeted ES clones (Figure 1b) were then injected into C57BL/6 blastocysts. As confirmed by Southern blotting, six chimeras derived from two independent ES clones showed germline transmission of the targeted allele (Figure 1c). Among the offspring of the clones, *ADAMTS-1*$^{+/-}$ heterozygotes were normal in appearance and were fertile. By crossbreeding heterozygotes, we obtained live *ADAMTS-1*$^{-/-}$ homozygotes. Using all conceivable RT-PCR primer sets as indicated in Figure 1a (top), we could not detect amplified bands from *ADAMTS-1*$^{-/-}$ templates; therefore, even truncated *ADAMTS-1* mRNA was not effectively transcribed in *ADAMTS-1*$^{-/-}$ mice. Figure 1d shows the result of RT-PCR using primer set (d).

Growth retardation in ADAMTS-1–null mice. *ADAMTS-1*$^{-/-}$ mice were smaller than their wild-type littermates, although their proportions were correct (Figure 2a). The reduction in body weight of *ADAMTS-1*$^{-/-}$ mice was already significant at birth, and was accentuated thereafter (Figure 2b): at 9 months the average body weight of *ADAMTS-1*$^{-/-}$ mice was only about 70% that of their wild-type or heterozygous littermates (Figure 2c). *ADAMTS-1*$^{-/-}$ mice were exceptionally lean, and the volume of epididymal fat was significantly smaller in *ADAMTS-1*$^{-/-}$ mice (Figure 2, d and e). Histological examination did not detect apparent changes in *ADAMTS-1*$^{-/-}$ adipose tissues except for the relatively small size of individual adipocytes (data not shown). Serum levels of nutritional indices were not significantly different between *ADAMTS-1*$^{-/-}$ and *ADAMTS-1*$^{+/+}$ males (respective values: total cholesterol, 92.0 ± 6.7 mg/dL vs. 100.3 ± 12.0 mg/dL, $n = 7$ in each; glucose, 174.7 ± 22.7 mg/dL vs. 168.1 ± 16.1 mg/dL, $n = 7$ in each; total protein, 4.5 ± 0.2 g/dL, $n = 10$ vs. 4.6 ± 0.4 g/dL, $n = 9$).

Urologic abnormalities in ADAMTS-1–null mice. The most prominent morphological feature of *ADAMTS-1*$^{-/-}$ mice was detected in the kidney. In 4-week-old

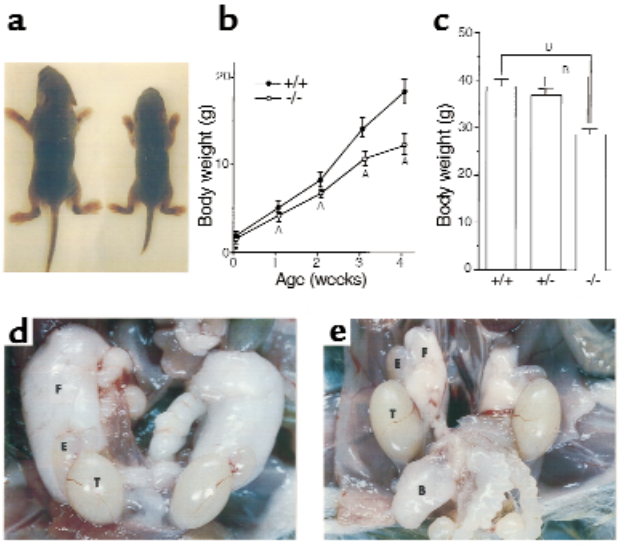

Figure 2
Growth retardation in *ADAMTS-1*$^{-/-}$ mice. (**a**) Appearance of 1-week-old *ADAMTS-1*$^{+/+}$ (left) and *ADAMTS-1*$^{-/-}$ (right) littermates. (**b**) Comparison of growth after birth between *ADAMTS-1*$^{+/+}$ ($n = 10$) and *ADAMTS-1*$^{-/-}$ ($n = 9$) littermates. $^{A}P < 0.05$ vs. wild-type littermates. (**c**) Comparison of body weight among 9-month-old *ADAMTS-1*$^{+/+}$, *ADAMTS-1*$^{+/-}$, and *ADAMTS-1*$^{-/-}$ littermates ($n = 13$ in each genotype). $^{B}P < 0.0001$. (**d** and **e**) Epididymal fat pads and testes from 12-week-old *ADAMTS-1*$^{+/+}$ (**d**) and *ADAMTS-1*$^{-/-}$ (**e**) littermates. B, bladder; E, epididymis; F, fat pad; T, testis.

Figure 3
Comparison of kidneys between *ADAMTS-1*$^{+/+}$ (**a**, **c**, **e**, **g**) and *ADAMTS-1*$^{-/-}$ (**b**, **d**, **f**, **h**, **i**) mice at 4 weeks. (**a** and **b**) Inner aspects of the kidneys. Arrow, renal papilla; arrowhead, fibrous tissue surrounding the ureteropelvic junction. (**c** and **d**) Hematoxylin and eosin–stained sections of the whole kidney. CS, caliceal space. (**e** and **f**) Mallory-azan–stained sections through the renal hilum; the ureteropelvic junction of *ADAMTS-1*$^{-/-}$ mice is rich in fibrous tissue (arrows). P, renal papilla. (**g**–**i**) Electron microscopy findings at the ureteropelvic junction in *ADAMTS-1*$^{-/-}$ mice and controls. (**h**) Excessive collagen fibers (arrows) between smooth muscle cells (Sm) at the ureteropelvic junction of *ADAMTS-1*$^{-/-}$ mice. (**i**) Thickening of the collagenous segment between the epithelial cell (Epi) layer and smooth muscle cell layer (12–30 μm), and proliferation of fibroblasts at the ureteropelvic junction of *ADAMTS-1*$^{-/-}$ mice. (**g**) Collagenous segment between the epithelial cell layer and smooth muscle cell layer (6–12 μm) from the ureteropelvic junction of normal mice. (**j**–**m**) Electron microscopy ureteral findings in *ADAMTS-1*$^{-/-}$ mice (**k**–**m**) and controls (**j**). (**k**) Thickening of the collagenous segment (arrows) between the epithelial cell layer and smooth muscle cell layer. (**l**) High magnification showing the accumulation of excessive collagen fibers in *ADAMTS-1*$^{-/-}$ mice. (**m**) Deformity and fissures (arrowheads) in smooth muscle cells in *ADAMTS-1*$^{-/-}$ mice. Bars in **e** and **f** represent 20 μm; bars in **g**–**m** represent 2 μm.

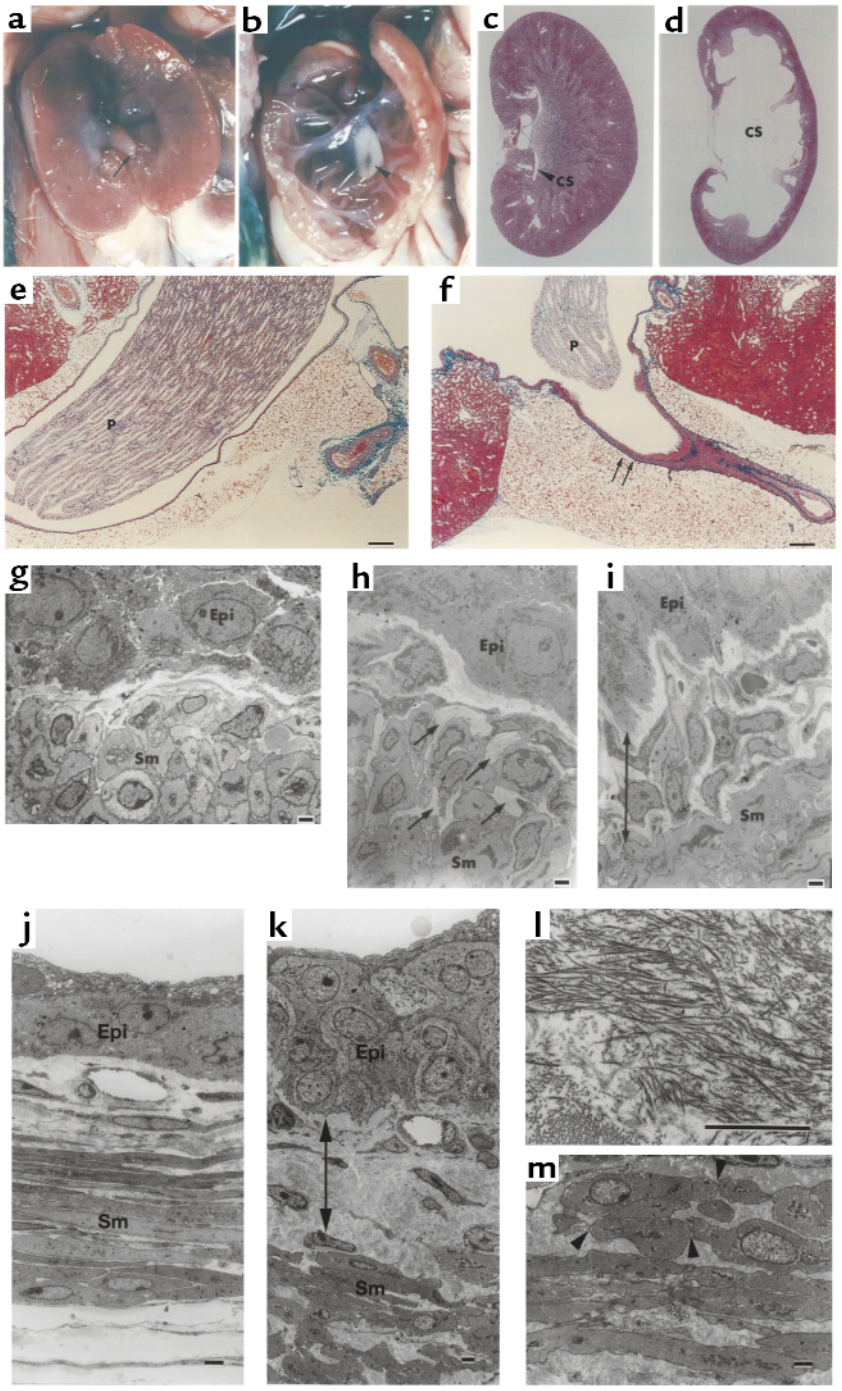

ADAMTS-1$^{-/-}$ mice, the caliceal space was greatly enlarged, and the corticomedullary tissue was severely reduced, forming a thin rim surrounding the enlarged calyx (Figure 3, a–d). In mice of both C57BL/6J and 129/Sv backgrounds, this defect was observed bilaterally with complete penetrance. The papillae of wild-type mice protruded beyond the hilum and filled most of the pelvic space, whereas the papillae of *ADAMTS-1*$^{-/-}$ mice were poorly developed or virtually absent (Figure 3, a–d). Electron microscopy showed degeneration of the collecting duct epithelial cells and interstitial fibrosis (data not shown). Slight but significant enlargement of the caliceal space with hypoplastic or atrophic papillae were first observed at around 1 week of age, suggesting that the renal phenotype appears after birth and develops progressively thereafter. As for renal function, we could detect no evidence of severe renal failure in *ADAMTS-1*$^{-/-}$ mice. Serum creatinine (Cr), blood urea nitrogen (BUN), and creatinine clearance (CCr) were not significantly different between *ADAMTS-1*$^{-/-}$ and *ADAMTS-1*$^{+/+}$ male mice (respective

values: Cr, 0.078 ± 0.006 mg/dL, n = 11 vs. 0.103 ± 0.022 mg/dL, n = 17; BUN, 25.6 ± 1.6 mg/dL, n = 16 vs. 26.4 ± 1.8 mg/dL, n = 12; CCr, 0.64 ± 0.09 mL/min, n = 6 vs. 0.70 ± 0.09 mL/min, n = 8). In contrast, the ability to concentrate urine was significantly compromised in *ADAMTS-1*$^{-/-}$ mice on a 0.7% NaCl diet compared with *ADAMTS-1*$^{+/+}$ mice, and urine volume was increased (2.37 ± 0.27 mL in –/– mice, n = 4 vs. 1.61 ± 0.12 mL in +/+ mice, n = 8; P < 0.05), whereas the specific gravity was decreased (1.054 ± 0.003, in –/– mice, n = 4 vs. 1.081 ± 0.004, in +/+ mice, n = 8; P < 0.001). In accordance with the increased urine volume, urinary concentrations of Na^+ (–/–, 90.1 ± 3.2 mEq/mL, n = 10 vs. +/+, 128.3 ± 4.3 mEq/mL, n = 10; P < 0.0001), K^+ (–/–, 249.2 ± 10.5 mEq/mL, n = 10 vs. +/+, 377.7 ± 15.7 mEq/mL, n = 10; P < 0.0001) and Cl^- (–/–, 126.9 ± 5.3 mEq/mL, n = 10 vs. +/+, 195.6 ± 7.7 mEq/mL, n = 10; P < 0.0001) were significantly lower in *ADAMTS-1*$^{-/-}$ mice than in *ADAMTS-1*$^{+/+}$ mice. After 2 weeks on a high-salt diet containing 8% NaCl, urine volume of *ADAMTS-1*$^{-/-}$ mice was increased by about two-fold over that of *ADAMTS-1*$^{+/+}$ mice (–/–, 11.72 ± 2.27 mL, n = 6 vs. +/+, 6.19 ± 0.78 mL, n = 6; P < 0.01). These anatomical and functional abnormalities are consistent with a state of hydronephrosis resulting from partial urinary obstruction (22).

The kidneys of *ADAMTS-1*$^{-/-}$ mice also exhibited retraction of the ureteropelvic junction inside the hilum, which was surrounded by fibrous tissue (Figure 3, a, b, e, and f). Electron microscopy revealed thickening of the collagenous segment between the epithelial cell layer and the smooth muscle cell layer in *ADAMTS-1*$^{-/-}$ mice (Figure 3, g–i). We further studied the histology of the ureter, and detected fundamentally the same type of abnormalities as seen in the ureteropelvic junction. As shown in Figure 3, k–l, accumulations of excessive collagen fibers were also found between the epithelial and smooth muscle cell layers in the ureteral specimens of *ADAMTS-1*$^{-/-}$ mice. Deformity and fissures were also detected in the smooth muscle cells in the ureter (Figure 3m). Thus, fibrotic changes diffusely involve the whole ureter in *ADAMTS-1*$^{-/-}$ mice.

Therefore, we performed intravenous pyelography to assess changes in urinary flow and to determine the extent to which the lesions could cause urinary obstruction. In wild-type mice, nephrograms and cystograms observed 5 minutes after injection of contrast medium showed both the calyces and pelvis to be smooth and pyramidal in shape (Figure 4a). By 30 minutes, the nephrograms had completely disappeared (Figure 4b). In *ADAMTS-1*$^{-/-}$ mice, the calyces were enlarged and distorted in shape, with a narrow pelvic space (Figure 4c). Washout of the contrast medium from the calyces was still incomplete after 30 minutes (Figure 4d).

Furthermore, ADAMTS-1 immunoreactivity was detected in the collecting ducts and (more intensely) in the urinary epithelium at the ureteropelvic junction (Figure 5). Taken together, the anatomical, radiographic, and immunohistochemical findings suggest that obstruction at the ureteropelvic junction may cause progressive caliceal enlargement.

Adrenal abnormalities in ADAMTS-1–null mice. *ADAMTS-1*$^{-/-}$ mice also showed adrenal glandular abnormalities. The adrenal medulla is normally composed of closely packed secretory cells supported by a fine reticular network containing numerous capillaries (Figure 6, a and c). In *ADAMTS-1*$^{-/-}$ mice, this structure was severely disrupted and contained numerous cavities (Figure 6, b and d). Remarkably, few capillaries containing blood cells were observed in the adrenal medulla of *ADAMTS-1*$^{-/-}$ mice (Figure 6, b and d). In contrast, there were no detectable abnormalities in the adrenal cortex of *ADAMTS-1*$^{-/-}$ mice. The urine levels of catecholamine metabolites were not different between *ADAMTS-1*$^{-/-}$ mice and *ADAMTS-1*$^{+/+}$ mice (respective values: metanephrine, 0.101 ± 0.021 μg/day, n = 4 vs. 0.097 ± 0.014 μg/day, n = 4; normetanephrine: 0.707 ± 0.101 μg/day, n = 4 vs. 0.518

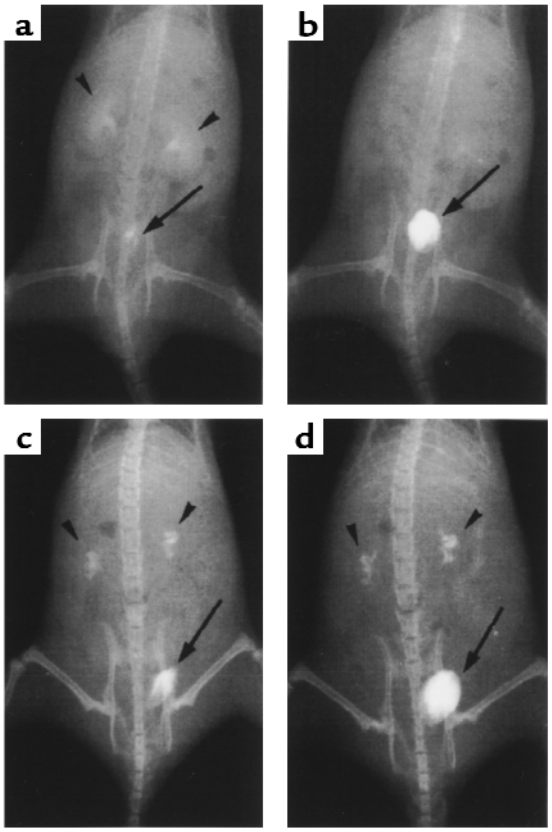

Figure 4
Intravenous pyelography (**a**–**d**). X-ray films were taken 5 minutes (**a** and **c**) and 30 minutes (**b** and **d**) after injection of contrast medium into 6-week-old *ADAMTS-1*$^{+/+}$ (**a** and **b**) and *ADAMTS-1*$^{-/-}$ (**c** and **d**) littermates. In *ADAMTS-1*$^{+/+}$ mice, normal nephrograms were detected at 5 minutes; these disappeared within 30 minutes. In *ADAMTS-1*$^{-/-}$ mice, the enlarged and distorted calyces still retained contrast medium after 30 minutes. Arrowheads and arrows indicate nephrograms and cystograms, respectively.

Figure 5
Immunohistochemistry of a mouse kidney section using an anti–ADAMTS-1 antibody (**a**) and a nonimmune control (**b**). J, urinary epithelium at the ureteropelvic junction. The pink staining shows the location of ADAMTS-1 expression in the urinary epithelium at the ureteropelvic junction.

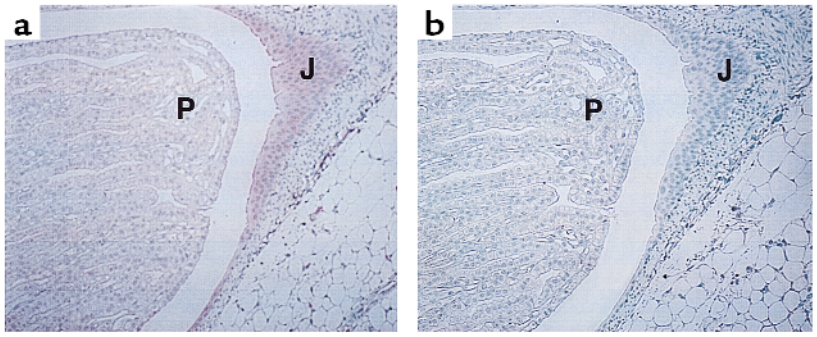

± 0.051 μg/day, $n = 4$), suggesting that the function of the adrenal medulla may not be seriously affected.

Abnormalities in female genital organs and impaired fertility in ADAMTS-1–null mice. Finally, *ADAMTS-1*$^{-/-}$ female mice showed abnormalities in the morphology of uterus and ovaries. The uterus of *ADAMTS-1*$^{-/-}$ females had a thick and convoluted shape (Figure 7b). In uterine sections of *ADAMTS-1*$^{-/-}$ females, extensive abnormal cystic formations were detected (Figure 7d). In addition, sections of ovary showed fewer numbers of mature follicles in *ADAMTS-1*$^{-/-}$ females (Figure 7f) than in *ADAMTS-1*$^{+/+}$ females.

In accordance with the anatomical changes, fertility was impaired in *ADAMTS-1*$^{-/-}$ females. When mated with males, *ADAMTS-1*$^{-/-}$ female mice characteristically experienced plug formation that was not followed by pregnancy. After mating with *ADAMTS-1*$^{-/-}$ males, only 13% of *ADAMTS-1*$^{-/-}$ females became pregnant after plug formation (5 pregnancies out of 40 detected plugs). On the other hand, more than 90% of *ADAMTS-1*$^{+/-}$ and *ADAMTS-1*$^{+/+}$ females became pregnant after plug formation. Even when *ADAMTS-1*$^{-/-}$ females became pregnant after breeding, the average number of pups was very small (2.5 ± 0.3, $n = 20$ vs. 10.4 ± 0.3 in +/+ mice, $n = 20$; $P < 0.001$). The number of implantation sites at 10 days after coitus was also reduced in *ADAMTS-1*$^{-/-}$ females (5.0 ± 0.8, $n = 4$ vs. 11.6 ± 0.7 in *ADAMTS-1*$^{+/+}$ mice, $n = 5$; $P < 0.01$). These data show that development of follicles, implantation, and intrauterine development may be affected in *ADAMTS-1*$^{-/-}$ female mice. Impaired fertility was observed only in females; *ADAMTS-1*$^{-/-}$ males sired both wild-type and heterozygous females normally.

Discussion

Data from *ADAMTS-1*–null mice obtained in this study show that ADAMTS-1 is necessary for normal growth and the structure and function of the kidneys, adrenal glands, and female reproductive organs. The lack of severe renal failure with azotemia or major metabolic disturbance suggests that the *ADAMTS-1* gene is pleiotropic, and that ADAMTS-1 has multiple and nonredundant functions throughout the body.

ADAMTS-1 is a member of the ADAM protein family that is involved in proteolytic modification of cell-surface proteins and extracellular matrices. The unique structure of ADAMTS-1, characterized by the presence of thrombospondin type I motifs, is shared by other newly identified proteins in mammals and in *C. elegans*, which constitute the ADAMTS subfamily that may perform well-conserved biological functions

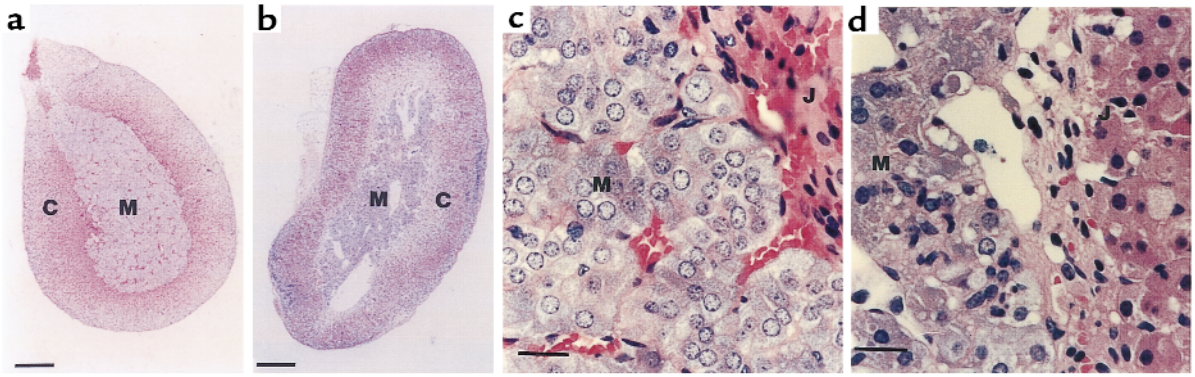

Figure 6
Comparison of the adrenal glands between *ADAMTS-1*$^{+/+}$ (**a** and **c**) and *ADAMTS-1*$^{-/-}$ (**b** and **d**) mice at 4 weeks of age. (**a** and **b**) Hematoxylin and eosin–stained sections of the adrenal glands. C, adrenal cortex; M, adrenal medulla. (**c**, **d**) High-magnification light micrographs of the adrenal medulla adjacent to the corticomedullary junction (J). Bars in **a** and **b** represent 20 μm; bars in **c** and **d** represent 200 μm.

(21). ADAMTS-1 is anchored to the extracellular matrix by an interaction between its carboxyl-terminal spacing region together with its thrombospondin type I motifs, and sulfated glycosaminoglycans such as heparan sulfate (14). ADAMTS-1 may, therefore, serve as a local factor processing as-yet unknown substrates by protease activity (15). It is notable that among the tissues we examined, the urinary epithelium at the ureteropelvic junction expressed the highest levels of ADAMTS-1 protein. The renal abnormalities involving the calyces and corticomedullary structure in *ADAMTS-1*$^{-/-}$ mice might be secondary to the structural abnormalities of the urinary tract. Thus ADAMTS-1 produced by the urinary epithelium may contribute to normal development or remodeling of the underlying fibrous tissue in the ureteropelvic junction and ureter.

Interestingly, mice lacking angiotensinogen, angiotensin-converting enzyme, or angiotensin type I receptor have a very similar renal phenotype (23–26). In these mice, hypoplastic ureteral smooth muscle and impaired ureteropelvic peristalsis are thought to cause functional obstruction of the urinary tract (23 and S. Okubo, personal communication). In contrast, *ADAMTS-1*$^{-/-}$ mice exhibit accumulation of excessive fibrous tissue and deformity of smooth muscle cells at the ureteropelvic junction and ureter, which could lead to both organic and functional obstruction. Electron microscopy showing the accumulation of collagen fibers suggests that processing of collagen and related matrix substances may be impaired in *ADAMTS-1*$^{-/-}$ mice. In this respect, it is noteworthy that ADAMTS-1 shares unique structural features with procollagen I N-proteinase and aggrecanase-1, other ADAM proteins that contain four thrombospondin type I motifs (16–18). This supports the notion that ADAMTS-1 may process collagen or related substrates (e.g., proteoglycans) that are important for the organization of organ structures.

The mechanisms responsible for growth retardation, female infertility with histological changes in the uterus and ovaries, and disrupted adrenomedullary architecture remain unknown. It is difficult to infer the molecular substrate or substrates of ADAMTS-1 that are common to the organs affected in knockout mice because the characteristics of histological changes seem to be different among organs. The discovery of physiologically relevant substrates of ADAMTS-1 would be expected to pave the way for further understanding of growth, fertility, and organ morphogenesis.

Recently, METH-1, the human orthologue of ADAMTS-1, was shown to suppress FGF-2–induced vascularization in the cornea pocket assay and to inhibit VEGF-induced angiogenesis in the chorioallantoic membrane assay (19). Consistent with this inhibitory effect on angiogenesis, METH-1 inhibits endothelial cell proliferation, but not fibroblast or smooth muscle growth (19). On the other hand, the lack of adrenomedullary capillary network formation in *ADAMTS-1*$^{-/-}$ mice suggests that ADAMTS-1 may be necessary for the capillary formation of the adrenal medulla. It is presently unclear how these contradictory findings could be reconciled. It is possible that the effect of ADAMTS-1 on angiogenesis may be different among tissues, developmental stages, and pathophysiological conditions. It is also possible that the lack of a capillary network in the adrenal medulla of *ADAMTS-1*$^{-/-}$ mice is not the direct effect of the *ADAMTS-1* null mutation. Further studies are necessary to clarify the role of ADAMTS-1 in angiogenesis and its molecular mechanism, which potentially involves extracellular matrices.

This study also has significant clinical implications. The renal phenotype of *ADAMTS-1*$^{-/-}$ mice resembles human ureteropelvic junction obstruction, which is the most common cause of congenital hydronephrosis and is recognized in nearly 1 in 500 live births (27). This disease is characterized by abnormal collagen and smooth muscle components at the ureteropelvic junction that contribute to mechanical or functional obstruction of urinary flow (27, 28). Interestingly, the structural abnormalities in *ADAMTS-1*$^{-/-}$ mice are responsible for the same dysfunctions described in cases of congenital

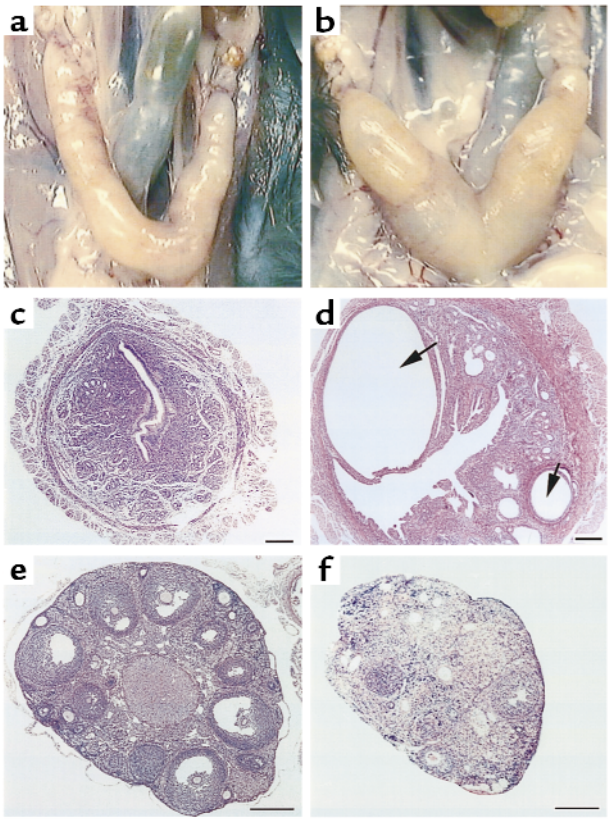

Figure 7
Comparison of uterus and ovary between *ADAMTS-1*$^{+/+}$ (**a**, **c**, **e**) and *ADAMTS-1*$^{-/-}$ (**b**, **d**, **f**) female mice at 12 weeks. (**a** and **b**) Exterior appearance of uterus and ovary. Hematoxylin and eosin–stained sections of uterus (**c** and **d**) and ovary (**e** and **f**). Arrows in **d** represent abnormal cystic formation in the uterus of *ADAMTS-1*$^{-/-}$ mice. Bars in **c**–**f** represent 100 μm.

ureteropelvic junction obstruction and primary obstructive megaureter in humans (29, 30). Thus, the *ADAMTS-1*–null mouse may represent a useful new disease model for clarification of the pathogenesis of congenital ureteropelvic junction obstruction.

Acknowledgments

We thank R.E. Hammer for SM-1 ES cells, P. Meneton for the Neo-tk plasmids, H. Iwasa for technical assistance, and W.F. Goldman for critical reading of the manuscript. Y. Kurihara is a Research Fellow of the Organization for Pharmaceutical Safety and Research, Japan. This work was supported by a Grant-in-Aid for Scientific Research from the Ministry of Education, Science and Culture, Japan (to H. Kurihara, Kouji Kuno, and H. Yokoyama) and by grants from the Cardiovascular Research Foundation, Tanabe Medical Frontier Conference, Suzuken Memorial Foundation, the Ryoichi Naito Foundation for Medical Research, and Tokyo Biochemical Research Foundation (to H. Kurihara).

1. Wolfsberg, T.G., Primakoff, P., Myles, D.G., and White, J.M. 1995. ADAM, a novel family of membrane proteins containing A Disintegrin And Metalloprotease domain: multipotential functions in cell-cell and cell-matrix interactions. *J. Cell Biol.* **131**:275–278.
2. Blobel, C.P. 1997. Metalloprotease-disintegrins: links to cell adhesion and cleavage of TNF alpha and Notch. *Cell.* **90**:589–592.
3. Blobel, C.P., et al. 1992. A potential fusion peptide and an integrin ligand domain in a protein active in sperm-egg fusion. *Nature.* **356**:248–252.
4. Almeida, E.A., et al. 1995. Mouse egg integrin alpha 6 beta 1 functions as a sperm receptor. *Cell.* **81**:1095–1104.
5. Yagami-Hiromasa, T., et al. 1995. A metalloprotease-disintegrin participating in myoblast fusion. *Nature.* **377**:652–656.
6. Moss, M.L., et al. 1997. Cloning of a disintegrin metalloproteinase that processes precursor tumour-necrosis factor-alpha. *Nature.* **385**:733–736.
7. Black, R.A., et al. 1997. A metalloproteinase disintegrin that releases tumour-necrosis factor-alpha from cells. *Nature.* **385**:729–733.
8. Peschon, J.J., et al. 1998. An essential role for ectodomain shedding in mammalian development. *Science.* **282**:1281–1284.
9. Buxbaum, J.D., et al. 1998. Evidence that tumor necrosis factor alpha converting enzyme is involved in regulated alpha-secretase cleavage of the Alzheimer amyloid protein precursor. *J. Biol. Chem.* **273**:27765–27767.
10. Rooke, J., Pan, D., Xu, T., and Rubin, G.M. 1996. KUZ, a conserved metalloprotease-disintegrin protein with two roles in Drosophila neurogenesis. *Science.* **273**:1227–1231.
11. Pan, D., and Rubin, G.M. 1997. Kuzbanian controls proteolytic processing of Notch and mediates lateral inhibition during Drosophila and vertebrate neurogenesis. *Cell.* **90**:271–280.
12. Kuno, K., et al. 1997. Molecular cloning of a gene encoding a new type of metalloproteinase-disintegrin family protein with thrombospondin motifs as an inflammation associated gene. *J. Biol. Chem.* **272**:556–562.
13. Kuno, K., Iizasa, H., Ohno, S., and Matsushima, K. 1997. The exon/intron organization and chromosomal mapping of the mouse ADAMTS-1 gene encoding an ADAM family protein with TSP motifs. *Genomics.* **46**:466–471.
14. Kuno, K., and Matsushima, K. 1998. ADAMTS-1 protein anchors at the extracellular matrix through the thrombospondin type I motifs and its spacing region. *J. Biol. Chem.* **273**:13912–13917.
15. Kuno, K., Terashima, Y., and Matsushima, K. 1999. ADAMTS-1 is an active metalloproteinase associated with the extracellular matrix. *J. Biol. Chem.* **274**:18821–18826.
16. Colige, A., et al. 1997. cDNA cloning and expression of bovine procollagen I N-proteinase: a new member of the superfamily of zinc-metalloproteinases with binding sites for cells and other matrix components. *Proc. Natl. Acad. Sci. USA.* **94**:2374–2379.
17. Prockop, D.J., Sieron, A.L., and Li, S.W. 1998. Procollagen N-proteinase and procollagen C-proteinase. Two unusual metalloproteinases that are essential for procollagen processing probably have important roles in development and cell signaling. *Matrix Biol.* **16**:399–408.
18. Tortorella, M.D., et al. 1999. Purification and cloning of aggrecanase-1: a member of the ADAMTS family of proteins. *Science.* **284**:1664–1666.
19. Vazquez, F., et al. 1999. METH-1, a human ortholog of ADAMTS-1, and METH-2 are members of a new family of proteins with angio-inhibitory activity. *J. Biol. Chem.* **274**:23349–23357.
20. Blelloch, R., and Kimble, J. 1999. Control of organ shape by a secreted metalloprotease in the nematode *Caenorhabditis elegans*. *Nature.* **399**:586–590.
21. Tang, B.L., and Hong, W. 1999. ADAMTS: a novel family of proteases with an ADAM protease domain and thrombospondin 1 repeats. *FEBS Lett.* **445**:223–225.
22. Sheehan, M.L., and Davis, J.C. 1959. Experimental hydronephrosis. *Arch. Pathol.* **68**:185–225.
23. Niimura, F., et al. 1995. Gene targeting in mice reveals a requirement for angiotensin in the development and maintenance of kidney morphology and growth factor regulation. *J. Clin. Invest.* **96**:2947–2954.
24. Okubo, S., et al. 1998. Angiotensinogen gene null-mutant mice lack homeostatic regulation of glomerular filtration and tubular reabsorption. *Kidney Int.* **53**:617–625.
25. Krege, J.H., et al. 1995. Male-female differences in fertility and blood pressure in ACE-deficient mice. *Nature.* **375**:146–148.
26. Miyazaki, Y., et al. 1998. Angiotensin induces the urinary peristaltic machinery during the perinatal period. *J. Clin. Invest.* **102**:1489–1497.
27. Koff, S.A., and Wise, H.A., II. 1996. Anomalies of the kidney. In *Adult and pediatric urology.* 3rd edition. J.Y. Gillenwater, J.T. Grayhack, S.S. Howards, and J.W. Duckett, editors. Mosby Inc. St. Louis, Missouri, USA. 2171–2196.
28. Murakumo, M., et al. 1997. Structural changes of collagen components and diminution of nerves in congenital ureteropelvic junction obstruction. *J. Urol.* **157**:1963–1968.
29. Hanna, M.K., Jeffs, R.D., Sturgess, J.M., and Barkin, M. 1976. Ureteral structure and ultrastructure. Part II. Congenital ureteropelvic junction obstruction and primary obstructive megaureter. *J. Urol.* **116**:725–730.
30. Gosling, J.A., and Dixon, J.S. 1978. Functional obstruction of the ureter and renal pelvis. A histological and electron microscopic study. *Br. J. Urol.* **50**:145–152.